Extreme Mechanics Letters 28 (2019) 1–7

Contents lists available at ScienceDirect

Extreme Mechanics Letters

journal homepage: www.elsevier.com/locate/eml

Architected materials for tailorable shear behavior with energy dissipation

Suihan Liu [a], Ali Imani Azad [b], Rigoberto Burgueño [a,b,*]

[a] Department of Mechanical Engineering, Michigan State University, 428 S Shaw Ln, East Lansing, MI 48824, USA
[b] Department of Civil & Environmental Engineering, Michigan State University, 428 S Shaw Ln, East Lansing, MI 48824, USA

ARTICLE INFO

Article history:
Received 27 November 2018
Received in revised form 23 January 2019
Accepted 26 January 2019
Available online 11 February 2019

Keywords:
Snap-through
Instabilities
Metamaterials
Energy dissipation
Shear deformation

ABSTRACT

A class of architected materials is proposed for tailorable shear behavior and high energy dissipation. Inclined beams with elastic snap-through instabilities define the microstructure of the proposed materials, which display a 'twinkling' phenomenon that converts strain energy to dynamic motions, resulting in rate-independent energy dissipation. The design concepts were experimentally validated using 3D printed prototypes under both half- and full-cycle shear deformation conditions, and shown to respond in rate-independent sequential snap-through transitions with large energy dissipation in the elastic regime. Numerical simulations and analytical analyses show that predictable material behavior and tunable shear properties can be designed through the microstructure's geometry. The proposed materials fill the need of dissipating energy under shear deformations in a recoverable and rate-independent manner.

1. Introduction

Energy dissipation, an important and desirable material property to be used in mechanical and civil engineering applications, consists of an irreversible energy loss in solids and structures as a result of the conversion of mechanical energy into heat [1]. The ability to dissipate energy enables materials to undergo large deformations at limited stresses, which is imperative for enhancing damage tolerance. The common mechanisms to achieve this goal, such as plastic yielding (associated with permanent deformations) and rate dependent viscosity, perform poorly under repetitive loading cycles or low strain-rate deformations. Recently, elastic instabilities are attracting increased attention for use as the fundamental mechanism in the design of energy dissipating/absorbing mechanical metamaterials [2–4] due to their rate-independent and motion-recoverable nature. Many material porotypes have realized this concept for uniaxial tension [5] or compression loading conditions [6–14], but little attention has been given to shear behavior.

Shear deformations often occurs in materials when subjected to relative in-plane motion. Materials that can dissipate energy under shear are necessary for public safety and personnel protection purposes, and could be deployed in applications such as helmets to prevent energy transfer to the brain due to glancing blows, backpacks to limit impact on the wearer, and civil structures to withstand ground motions. An example of energy dissipating materials under shear is the use of elastomeric cellular struts to obtain tailorable compression and shear responses with negative stiffness [15]. Negative stiffness results from an unstable response as the reaction force acts in the same direction as the deformation, which helps the deformation increase without requiring additional external work. Thus, negative stiffness is a useful property that can release a system's stored strain energy, limit stresses, and allow for large deformations [16–18].

Here, we report a new class of architected material consisting of periodic snapping elements with controllable energy dissipation properties under shear, which are governed by the architecture of the material microstructure. The design concept is illustrated in Fig. 1. Elastic inclined beams were chosen as the unit elements, which can experience limit-point snap-through instability under vertical displacement. The limit point is an inflection of the primary equilibrium path that causes a stiffness change from stable to unstable. This transition corresponds to a negative stiffness region, which leads to a rapid unstable motion that triggers a release of the system's stored strain energy and is reflected in the energy-deformation curve as a loss of convexity. The unstable transition stops when the system reaches its next closest stable equilibrium path, and the rate of the motion is independent from the external deformation/load rate if it is not constrained by the system's boundary conditions.

A single inclined beam element under end shear deformation exhibits a negative stiffness region but follows the same load-deformation path upon unloading with no energy dissipation (Fig. 1a). The proposed structures (see Fig. 1b) consist of an array

* Corresponding author at: Department of Civil & Environmental Engineering, Michigan State University, 428 S Shaw Ln, East Lansing, MI 48824, USA.
E-mail address: burgueno@msu.edu (R. Burgueño).

https://doi.org/10.1016/j.eml.2019.01.010
2352-4316/

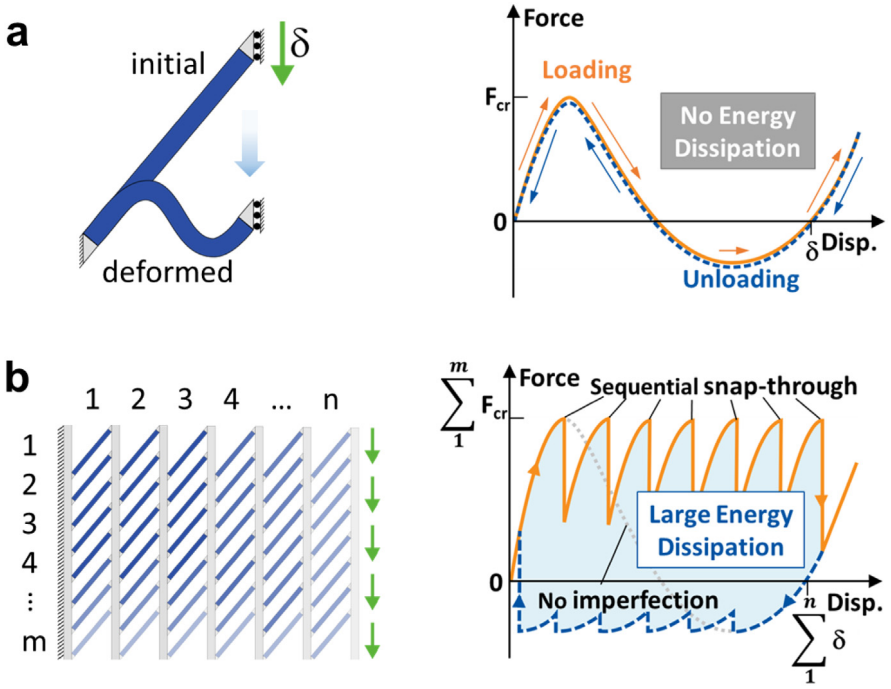

Fig. 1. Schematic of snapping element(s) and their force–displacement response. (a) A single unit elastic snapping beam element in its initial and deformed configuration (left), and its response curve under applied displacement with a negative stiffness region but no energy dissipation (right). (b) An array of $m \times n$ connected units (left) and its sequential snap-through response curve under an applied displacement with energy dissipation (right), where the gray dotted line shows the response of the system when there is no imperfection.

of $m \times n$ beam units, with m units that are equally spaced in a vertical stack (rows) and rigidly connected to end-constraining segments, and n repeating columns of the multi-row beam assemblies. Under in-plane shear motion, the beam units within a column respond simultaneously with the critical force being simply the summation of the individual critical forces of the m elements in the column. Given the unavoidable geometric imperfections in the system, the n coupled columns in series connection respond in sequential snap-through transitions, with the force–displacement response displaying n 'jumps' and n unstable paths, and the total deformation is equal to the summation of the displacements from the n columns. Since the 'jumps' are due to unstable transitions of the beams within a column, the unit elements are able to experience unbounded motions between the two stable equilibrium states until the motion decays due to friction. Energy dissipation consequently occurs by the release of mechanical energy, through the unstable snap-through motions, and its conversion to kinetic energy and in turn into heat. This phenomenon has been termed 'twinkling' and can be modeled by a spring–mass chain with non-monotonic stiffness elements that permit oscillatory behavior of the inner masses [19–21].

The material structures (Fig. 2a) consist of elastic beam unit segments and rigid (much higher material stiffness) end-constraining segments. The rigid end-constraining segments feature a linear sliding mechanism at their ends (top and bottom) to allow relative vertical movement between adjacent columns but prevent lateral motion of the beam elements within a column. Structure prototypes were fabricated using a 3D polymer printer (Objet350 Connex3, Stratasys Ltd., Eden Prairie, MN) that allows monolithic multi-material printing by jetting microscopic layers of liquid photopolymer and instantly curing them with UV light. A soft rubber-like polymer (TangoBlackPlus) was used for the elastic beam segment and a stiff polymer (VeroWhite) was used for the rigid end-constraining segments. The initial and deformed configuration of a 3D printed unit under vertical displacement (shear deformation) are shown in Fig. 2b.

The effects of the two dominant parameters, initial angle θ and slenderness t/L, on the mechanical response of single inclined beams has been numerically investigated [6] with the aim of characterizing their energy trapping or energy restoring features. Based on the noted study, two beam geometries ($\theta = 25°$, $t/L = 0.17$ and $\theta = 40°$, $t/L = 0.18$) were used as the unit elements for all the test prototypes considered in this study; with all beam elements having constant 20 mm depth (d) and 7 mm length (L). Two single-beam unit elements with the noted geometries were 3D printed and tested to verify their snap-through behavior.

For the proposed energy-dissipating material system, consisting of multiple-unit structures, all beams in the array had the same geometry and each column of beam elements deforms in a predefined direction. Two multiple-unit design layouts, differing in the arrangement of the columns' beam orientation, were designed to operate under half-cycle (i.e., only positive loading–unloading) and full-cycle (i.e., positive and negative loading–unloading) cyclic in-plane shear demands (see Figure S2 in the Supporting Information). The three 3D printed material prototypes for the half- and full-cycle design layouts are shown in Figs. 2c and 2d, respectively.

2. Results and discussions

We performed experiments on two 3D printed single-beam units and three multiple-unit structures (Figs. 2c and 2d) to characterize their shear behavior and showcase the design concept under both half- and full-cycle loading. The tested structures were initially placed in their undeformed states, and the in-plane shear deformation was applied as a relative vertical displacement along one edge of the test sample with respect to the other fixed edge. Testing was conducted at three deformation rates: 5 mm/s, 10 m/s and 15 mm/s.

The mechanical responses of the single-beam units are shown in Figs. 3a and 3b. To better compare between different structure geometries, a stress measure was calculated by normalizing the reaction force by the number of beam elements in the columns

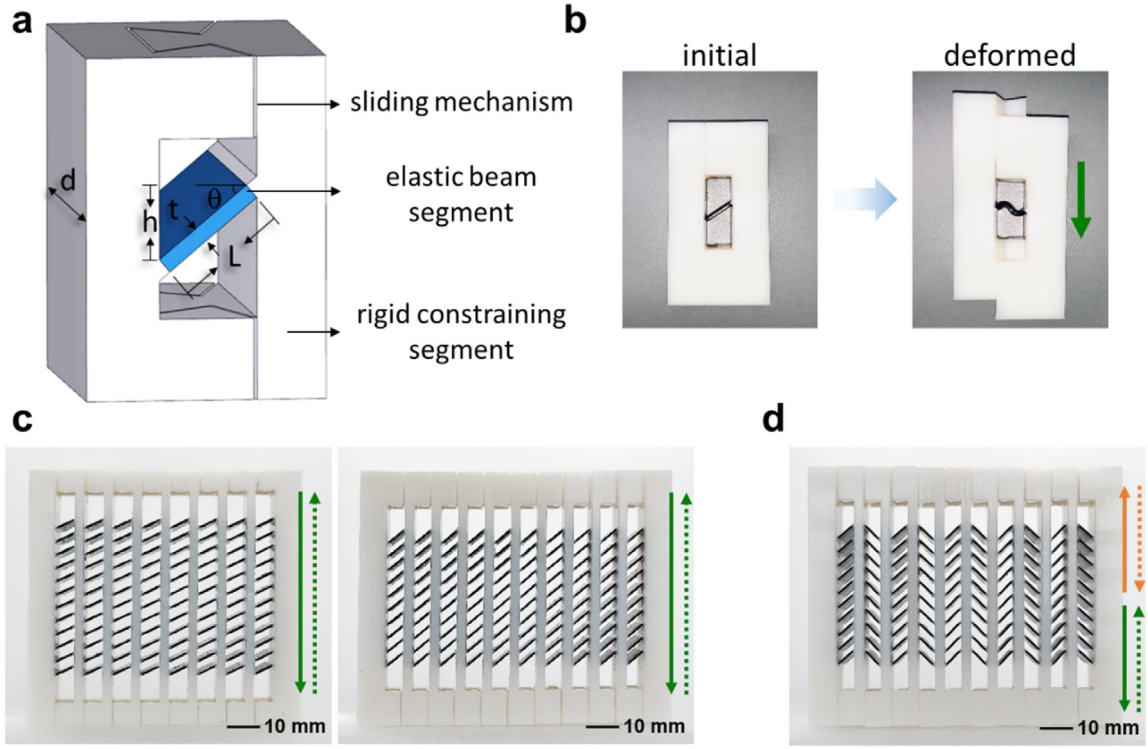

Fig. 2. Proposed material structures. (a) Schematic of the proposed material model for a unit element. (b) Initial and deformed configurations of a 3D printed single-beam unit. (c) 3D printed material prototypes for half-cycle loading condition (left: $\theta = 25°$, $t/L = 0.17$, m, $n = 12, 8$; right: $\theta = 40°$, $t/L = 0.18$, m, $n = 10, 10$). (d) 3D printed material prototypes for full-cycle loading condition ($\theta = 40°$, $t/L = 0.18$, m, $n = 10, 5 \times 2$). Note: solid and dashed lines indicate loading and unloading directions, respectively.

(i.e., m) and their unit geometry; and the strain is the displacement normalized by the maximum displacement applied during the test (Δ_{max}). Two observations are noted. First, the response curves of both units are consistent for the different deformation rates, which is indicates small rate effect from the viscoelastic nature of the polymer material in the 3D printed samples. Second, there is a small deviation between the loading and unloading paths. From experimental observation, this deviation is due to unavoidable eccentricity of the alignment between the loading frames when shear deformation was applied (see Figure S1 in the Supporting Information), but the resulting enclosed areas are small and it is not considered to contribute towards energy dissipation in the system.

The two multiple-unit structures in Fig. 2c were also loaded at the three noted deformation rates, and the measured shear stress–strain responses for the $\theta = 25°$ and $\theta = 40°$ systems are shown in Figs. 3c and 3d, respectively. It is immediately obvious that, unlike the single-beam units, the multi-unit structures display hysteretic force–deformation responses with a large enclosed areas and thus energy dissipating capacity. Under the applied shear deformation, the beam elements within the columns deform simultaneously and snap to their deformed state once their critical stress is reached. Due to manufacturing imperfections one beam will reach its critical stress first, and this effect will lead to one column reaching essentially simultaneous snap-through buckling of all its beams. This deformation process is passed on to another column as loading proceeds. The applied shear deformation was stopped when all columns switched to their buckled configuration. The test unit was then unloaded by reversing the deformation to the initial position and the structure snapped back column by column during this process until all columns (and their beams) returned to their initial undeformed configuration in sequential snap-through motions. Because of manufacturing imperfections, the snap-through sequence of the columns may vary in different loading cycles. Sequential images at different strains of the deformation response of the one half-cycle structure ($\theta = 25°$, $t/L = 0.17$, m, $n = 12, 8$) due to the applied shear during loading and unloading are shown in Fig. 3e. The full deformation process of both half-cycle structures (Fig. 2c) can be seen in Videos S1 and S2 in the Supporting Information.

For a given base material, the critical stress limit is determined by the beam unit geometry. Figs. 3c and 3d show that the structure with $\theta = 25°$, $t/L = 0.17$ has average peaks around 20 MPa and the structure with $\theta = 40°$, $t/L = 0.18$ has average peaks around 40 MPa, which are consistent with the responses of the corresponding single-beam geometry, in Figs. 3a and 3b. As each column snaps-through at the critical stress limit, it results in a peak on the stress–strain curve and followed by a negative stiffness region. The system regains a positive stiffness as the load resisted by the un-buckled columns provide a stable equilibrium path until another undeformed column reaches its critical stress limit. Thus, the number of units in a row, or number of columns, (i.e., n) controls the number of peaks and the unstable regions in the response. Ideally all the peaks in the response should be identical since the columns are in a series connection that deforms sequentially (one at a time) under the applied end displacement, and the columns that experience snap-through buckling should not deform further as the total displacement increases. However, gravity and friction resistance at the sliding mechanisms on the rigid end-constraining segments affect the experimental response and lead to additional displacement transfer to the snapped columns that deforms them beyond their snapped state. These factors in the experiments added a stiffening effect on the response curves and also resulted in a residual force on the structure when the applied displacement was removed. Nonetheless, it is clear the responses are repeatable and stable under cyclic shear loading, and that their behavior is characterized by the structures' unit geometry and the number of units in series connection (n).

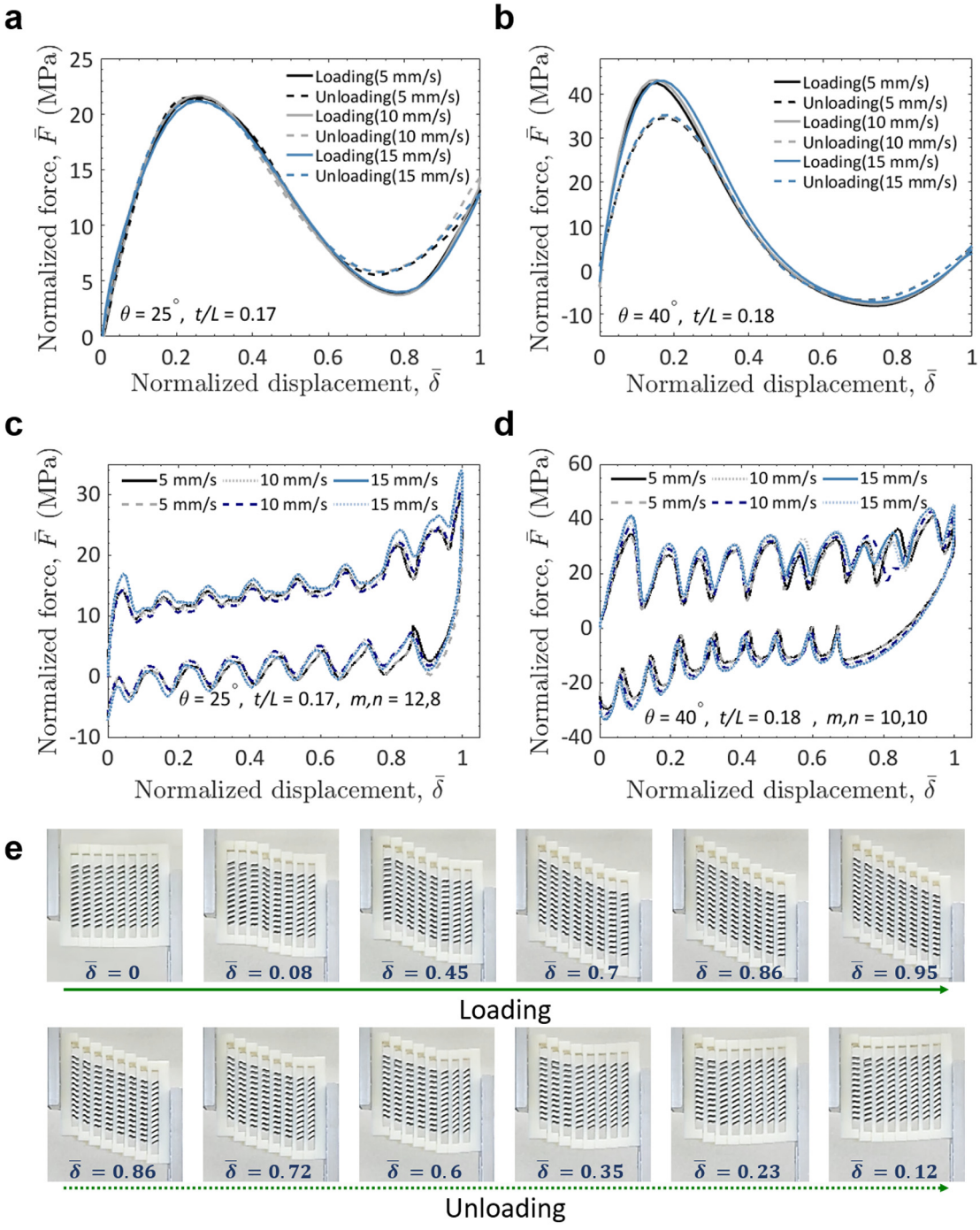

Fig. 3. Experimental results of single beam units and multiple-unit material prototypes for half-cycle shear loading condition. (a) Stress–strain response of single beam (θ = 25°, t/L = 0.17). (b) Stress–strain response of sample (θ = 40°, t/L = 0.18). (c) Stress–strain response of sample (θ = 25°, t/L = 0.17, m, n = 12, 8). (d) Stress–strain response of sample (θ = 40°, t/L = 0.18, m, n = 10, 10). (e) Sequential deformation process of sample (θ = 25°, t/L = 0.17, m, n = 12, 8) under a shear loading/unloading cycle. All samples were loaded at various strain rates (5 mm/s, 10 mm/s, and 15 mm/s). Note: the normalized force (stress) $\bar{F}$ equals to FL^3/mIh, and the normalized displacement (strain) is defined as $\Sigma\delta/\Delta_{max}$.

The polymer material used for the elastic beam units (TangoBlackPlus) is known to have hyperelastic behavior (see Figure S4 in the Supporting Information). However, the mechanism used in the proposed design concept to realize energy dissipation is based on the 'twinkling' phenomena and not the viscoelastic nature of the base material. This is confirmed by noting from Figs. 3c and 3d that there is only a small difference between the response curves of the multiple-unit structures (Fig. 2c) when tested at different strain rates. While the small differences in the responses can be attributed to the viscoelasticity of the base material, its effect is small and it can be concluded that proposed energy dissipation mechanism is preserved without any viscous material effects. This is supported by the analytical model presented later in this paper. Thus, the shear stress–strain response of the designed material system is dependent on its architecture but independent from the external loading rate.

In the material structures designed for a half-cycle condition, the shear deformation takes place in a single direction, and the response cycle only occurs in the positive domain of the stress–strain diagram. The deformation process of the full-cycle structure

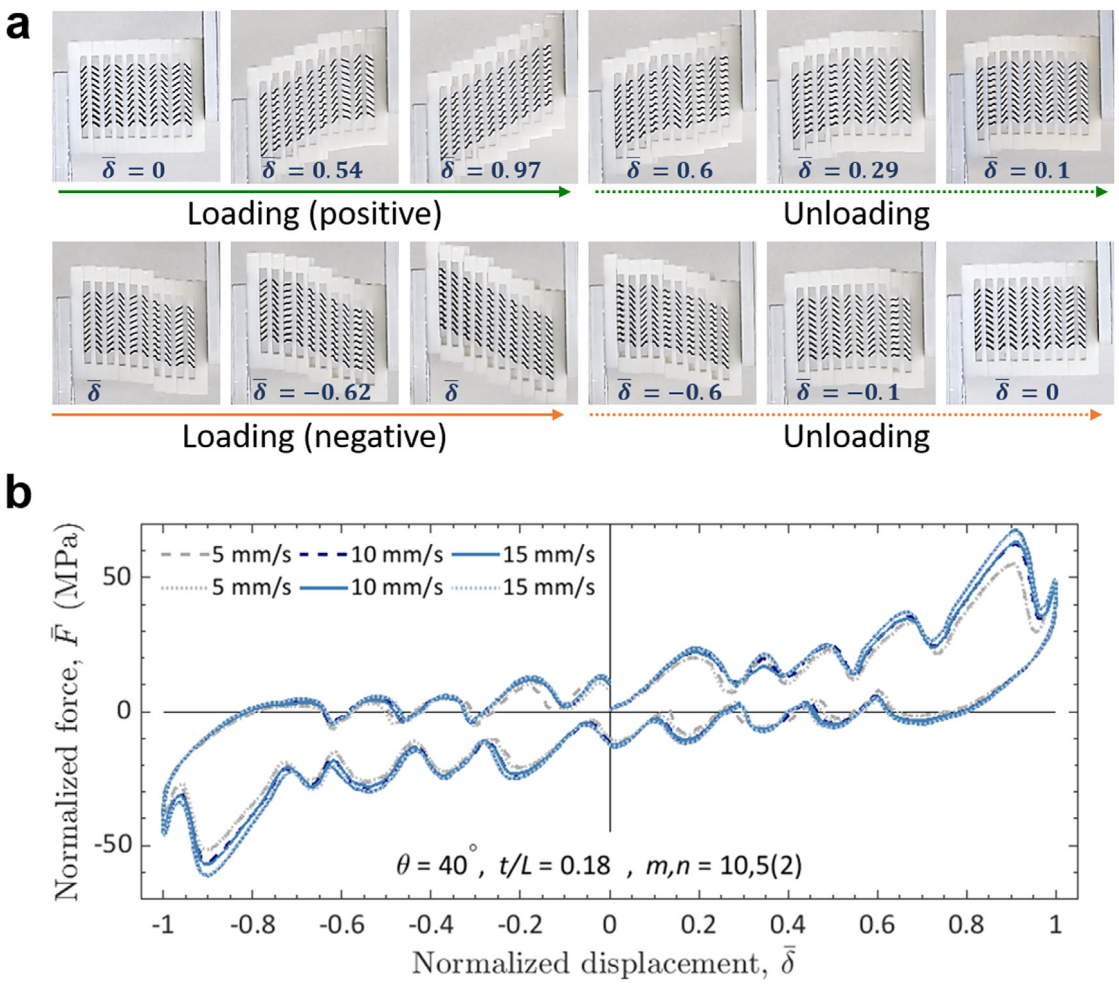

Fig. 4. Experimental results of a multiple-unit material prototype for full-cycle shear loading condition ($\theta = 40°$, $t/L = 0.18$, m, $n = 10, 5\times2$). (a) Sequential deformation process of the sample under a full-cycle of shear deformation. (b) Stress–strain response of the sample at various strain rates. All samples were loaded at various strain rates (5 mm/s, 10 mm/s, and 15 mm/s). Note: the normalized force (stress) $\bar{F}$ equals to FL^3/mlh, and the normalized displacement (strain) is defined as $\Sigma\delta/\Delta_{max}$.

prototype (Fig. 2c), for which a fully-reversed shear deformation cycle takes place, is shown in Fig. 4a. Of the ten columns in this structure, five have their beam units tilted to permit deformation in one direction while the other five feature a beam inclination that allows deformation in the other direction, and the columns are alternatively arranged to allow fully reversed cyclic loading within a single structure. Under an applied displacement, the columns with beams aligned with the active loading direction deform in a sequential manner while the columns with beams aligned in the opposite direction remain at their undeformed states. The same deformation process is followed by the columns with oppositely aligned beams when loading reverses to the other direction (see Video S3 in the Supporting Information). Each loading direction activates snap-through instabilities in five columns, which leads to five jumps in the stress–strain curves in both the positive and negative domains; and generates a hysteresis area that covers the entire response diagram. This sample was also tested at three different deformation rates and the shear stress–strain responses are shown in Fig. 4b. As learned from the half-cycle test units, the response was also repeatable and rate-independent under full-cycle shear deformations.

The experimental results revealed that the shear behavior of the proposed structures is characterized by the inclined beam unit geometry and the number of coupled columns (n). To further explore the effect of beam unit geometry on the performance of the proposed material systems, finite element (FE) analyses were conducted using the program ABAQUS. Dynamic analyses were conducted using the program's implicit solver with consideration of large deformations under quasi-static conditions. The 2D continuum-type element CPE4 was used assuming plane strain conditions, and artificial imperfection was introduced to the system through mesh variation at one randomly selected beam unit in each column. For the single unit system, only the elastic beam element was modeled and each beam was deformed by applying a vertical displacement to one of the ends and fixing all motions of the other end. Out-of-plane movements were constrained. For the multiple-unit system, both the elastic beams and rigid constraining segments were modeled and their adjoining surfaces were constrained to each other (tie). A friction coefficient was assigned to the contacting surfaces that modeled the linear sliding mechanisms at the ends of the constraining columns. The response of the rubber-like polymer was simulated using a visco-hyperelastic model (Figure S4 in the Supporting Information); and an elastic modulus of 2300 MPa and Poisson's ratio of 0.3 were used for the stiff polymer material.

The numerical and experimental stress–strain responses of two structures with multiple units ($\theta = 25°$, $t/L = 0.17$, m, $n = 12$, 8 and $\theta = 40°$, $t/L = 0.18$, m, $n = 10$, 10) are compared in Fig. 5a. The numerical simulation takes into consideration the friction between the rigid constraining segments when the structures open up on loading, and is considered to be in good agreement with the experimental traces. However, the numerical simulations become

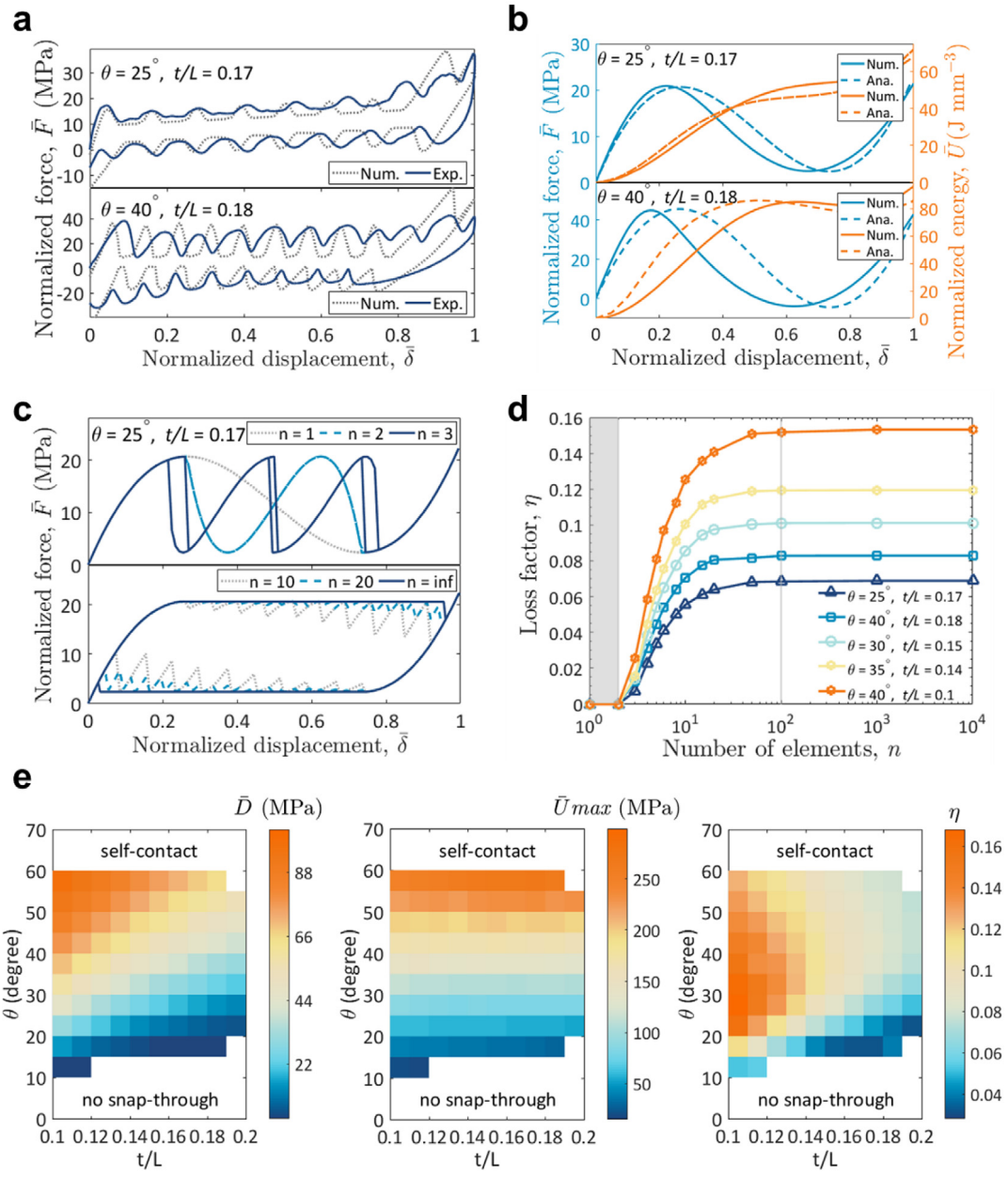

Fig. 5. Effect of the architecture on the response of the proposed material structures. (a) Experimental and numerical stress–strain response for two multiple-unit structures for $\theta = (25°, 40°)$, $t/L = (0.17, 018)$, and $m, n = (12, 8; 10, 10)$. (b) Numerical and analytical stress and strain energy responses for two unit beams for $\theta = (25°, 40°)$ and $t/L = (0.17, 0.18)$. The normalized strain energy equals to $UL^3/mnIh$ with the unit in MPa or J/mm^3. (c) Effect of n on the stress–strain response for a given unit geometry ($\theta = 25°$, $t/L = 0.17$) . (d) Effect of unit geometry on energy dissipation efficiency for five unit beams for $\theta = (25°, 40°, 30°, 35°, 40°)$ and $t/L = (0.17, 0.18, 0.15, 0.14, 0.1)$. (e) Parametric study of beam unit geometry on the energy properties of the proposed structures.

computational expensive when the number of unit elements increases and were further used only for predicting single element response. Thus, a simplified analytical model was used to explore the effect of number of unit elements n on the material structure behavior for a given unit geometry. Fig. 5b compares numerical and analytical results of the stress–strain and strain energy responses of single elements with $\theta = 25°$ and $\theta = 40°$. It can be seen that the negative stiffness region caused by a release of the system stored strain energy is reflected as a non-convex energy curve. The simplified model can qualitatively capture the snap-through behavior of the unit beams in terms of critical forces, as well as the maximum and minimum energy; which is adequate to predict the multi-unit system response for a given material architecture.

The effect of n on the amount of energy dissipated in the structure was explored analytically using unit elements with $\theta = 25°$ and $t/L = 0.174$. The force–deformation response for a half-cycle shear loading condition is presented in Fig. 5c. It can be seen that when the number of units is lower than 3, the loading and unloading paths are coincident, with negative stiffness regions but no energy dissipation. This response follows from the fact that the unstable motion of the unit's DOFs (degrees-of-freedom) are imposed/stabilized by the applied deformation and the boundary conditions. When n increases to 3, the middle element's DOF is free to be unstable under the applied displacement, which leads to energy dissipation of the system — as seen by the areas defined by the different loading and unloading paths. As n is further increased, more DOFs from the inner connected elements are free to experience unstable response, which leads to higher energy dissipation reflected as an enlarged hysteresis area. The distance (deformation) between the unstable 'jumps' in the response curve

reduces as more stable equilibrium paths are provided by the increased number of elements in the system, which will eventually result in a smooth response curve that encloses a region defined by two flat horizontal lines at the critical stress values and the two stable equilibrium paths. This leads to an elastic–plastic-type behavior [22,23] of the proposed structures that is recoverable.

Taking into consideration the work energy imposed to the system, energy dissipation efficiency can be quantified by the loss factor, $\eta = \overline{D}/\pi\overline{U}_{max}$, where $\overline{D}$ is the dissipated energy per loading–unloading cycle (area enclosed by the $\overline{F}-\overline{\delta}$ curve), $\overline{U}_{max}$ is the strain energy at Δ_{max}, and π is used instead of 2π since only the positive stress–strain cycle is considered in this case (since the cyclic integral extends only over a half cycle.) The loss factor for material systems with five different unit beam geometries are presented as a function of n in Fig. 5d. The effect of system architecture on the stress–strain response of the structures can also be observed by the η-n curves. The results show that no energy dissipation occurs, and η equals to zero, when n is less than three (i.e., gray region in Fig. 5d). As n increases beyond three η has a dramatic growth with increasing n and keeps rising towards a plateau. When n exceeds 100, η stabilizes at a plateau value based on the unit geometry and becomes independent of n. This plateau is reached as the loading and unloading paths in the stress–strain response of a multi-unit material structure become two horizontal lines at the critical snap-buckling stresses, leading to the maximum hysteresis area. From the η-n diagram, we can see that once the number of units reaches a 'saturation' point the optimal energy dissipating performance of the proposed material structures is solely based on the beam unit geometry.

Properties of the proposed material systems at their optimal condition for a given unit geometry can be calculated and the numerical results are shown in Fig. 5e. The response map covers a wide range of unit geometries through combinations of θ and t/L, and the resulting properties are shown in terms of normalized dissipated energy $\overline{D}$, normalized maximum strain energy $\overline{U}_{max}$, and loss factor η. The raw data used to generate this map can be found in Tables S1, S2 and S3 in the Supporting Information.

A beam element experiences no snap-through instability when the value of θ is too low (i.e., the beam is close to perpendicular to the applied displacement direction), and self-contact due to large deformation occurs when the value of θ is too high (i.e., the beam is close to parallel to the applied displacement direction). These two conditions, indicated as white regions in Fig. 5d, define the feasible design domain of the material structures — colored area in the figure. Within the design domain, the system dissipates more energy as θ increases and t/L decreases, as a result of the increased absolute difference between the two critical snap-through stresses (see Fig. S5 in the Supporting Information). Also, the maximum strain energy due to the applied shear deformation increases as both θ and t/L increase. This narrows the map that leads to high loss factor to the left middle region, which gives the highest η equal to 0.167 for a unit beam element with $\theta = 25^\circ$ and $t/L = 0.1$.

3. Conclusions

In summary, we have demonstrated the ability to tailor shear response with controllable energy dissipation in a new class of 3D printed architected material by combining experiments, simulations, and analyses. The proposed materials offer recoverable and rate-independent response under cyclic shear deformations by utilizing the unique response of elastic instabilities in their microstructure. Design of the material's periodic architecture allows independent control of the critical stress limit and the energy dissipation properties, and permits the material structures to be functional under both half- and full-cycle in-plane shear deformations. The amount of dissipated energy in these materials depends solely on the microstructural geometry once the number of unit elements reach saturation, and their response is highly predictable. These mechanical metamaterial may find applications in mechanical engineering for protective equipment and packaging, or civil systems for infrastructure safety under a variety of shear loading conditions.

Acknowledgments

The presented work was carried out with support from the U.S. National Science Foundation under grant numbers ECCS-1408506, CMMI-1463164 and CMMI-1762119. S.L. and R.B. designed the research and wrote the paper; S.L. and A.A performed the research; S.L. and R.B. analyzed the data.

Appendix A. Supplementary data

Supplementary material related to this article can be found online at https://doi.org/10.1016/j.eml.2019.01.010.

References

[1] T.L. Bergman, F.P. Incropera, D.P. DeWitt, A.S. Lavine, Fundamentals of Heat and Mass Transfer, John Wiley & Sons, 2011.
[2] N. Hu, R. Burgueño, Buckling-induced smart applications: recent advances and trends, Smart Mater. Struct. 24 (6) (2015) 063001.
[3] K. Bertoldi, Harnessing instabilities to design tunable architected cellular materials, Ann. Rev. Mater. Res. (2017).
[4] D. Kochmann, K. Bertoldi, Exploiting microstructural instabilities in solids and structures: from metamaterials to structural transitions, Appl. Mech. Rev. (2017).
[5] A. Rafsanjani, A. Akbarzadeh, D. Pasini, Snapping mechanical metamaterials under tension, Adv. Mater. 27 (39) (2015) 5931–5935.
[6] S. Shan, S.H. Kang, J.R. Raney, P. Wang, L. Fang, F. Candido, J.A. Lewis, K. Bertoldi, Multistable architected materials for trapping elastic strain energy, Adv. Mater. 27 (29) (2015) 4296–4301.
[7] R.L. Harne, Y. Song, Q. Dai, Trapping and attenuating broadband vibroacoustic energy with hyperdamping metamaterials, Extreme Mech. Lett. 12 (2017) 41–47.
[8] C.S. Ha, R.S. Lakes, M.E. Plesha, Design, fabrication, and analysis of lattice exhibiting energy absorption via snap-through behavior, Mater. Des. (2018).
[9] L. Wu, X. Xi, B. Li, J. Zhou, Multi-stable mechanical structural materials, Adv. Energy Mater. (2017).
[10] D.M. Correa, T. Klatt, S. Cortes, M. Haberman, D. Kovar, C. Seepersad, Negative stiffness honeycombs for recoverable shock isolation, Rapid Prototyping J. 21 (2) (2015) 193–200.
[11] D.M. Correa, C.C. Seepersad, M.R. Haberman, Mechanical design of negative stiffness honeycomb materials, Integr. Mater. Manuf. Innov. 4 (1) (2015) 1–11.
[12] T. Frenzel, C. Findeisen, M. Kadic, P. Gumbsch, M. Wegener, Tailored buckling microlattices as reusable light-weight shock absorbers, Adv. Mater. 28 (28) (2016) 5865–5870.
[13] C. Findeisen, J. Hohe, M. Kadic, P. Gumbsch, Characteristics of mechanical metamaterials based on buckling elements, J. Mech. Phys. Solids 102 (2017) 151–164.
[14] D. Restrepo, N.D. Mankame, P.D. Zavattieri, Phase transforming cellular materials, Extreme Mech. Lett. 4 (2015) 52–60.
[15] E.B. Duoss, T.H. Weisgraber, K. Hearon, C. Zhu, W. Small I.V., T.R. Metz, J.J. Vericella, H.D. Barth, J.D. Kuntz, R.S. Maxwell, Three-dimensional printing of elastomeric, cellular architectures with negative stiffness, Adv. Funct. Mater. 24 (31) (2014) 4905–4913.
[16] R. Lakes, Extreme damping in composite materials with a negative stiffness phase, Phys. Rev. Lett. 86 (13) (2001) 2897.
[17] R. Lakes, W. Drugan, Dramatically stiffer elastic composite materials due to a negative stiffness phase? J. Mech. Phys. Solids 50 (5) (2002) 979–1009.
[18] R.S. Lakes, T. Lee, A. Bersie, Y. Wang, Extreme damping in composite materials with negative-stiffness inclusions, Nature 410 (6828) (2001) 565.
[19] B.F. Feeny, A.R. Diaz, Twinkling phenomena in snap-through oscillators, J. Vib. Acoust. 132 (6) (2010) 061013.
[20] A.M. Balk, A.V. Cherkaev, L.I. Slepyan, Dynamics of chains with non-monotone stress–strain relations. I. Model and numerical experiments, J. Mech. Phys. Solids 49 (1) (2001) 131–148.
[21] A.M. Balk, A.V. Cherkaev, L.I. Slepyan, Dynamics of chains with non-monotone stress–strain relations. II. Nonlinear waves and waves of phase transition, J. Mech. Phys. Solids 49 (1) (2001) 149–171.
[22] I. Müller, P. Villaggio, A model for an elastic–plastic body, Arch. Ration. Mech. Anal. 65 (1) (1977) 25–46.
[23] G. Puglisi, L. Truskinovsky, Mechanics of a discrete chain with bi-stable elements, J. Mech. Phys. Solids 48 (1) (2000) 1–27.